

RESEARCH

Open Access



Biochar synthesis from mineral and ash-rich waste biomass, part 2: characterization of biochar and co-pyrolysis mechanism for carbon sequestration

Rahul Ramesh Nair^{1*} , Patrick A. Kißling², Alexander Marchanka³, Jacek Lecinski⁴, Ariel E. Turcios⁵, Madina Shamsuyeva⁴, Nishanthi Rajendiran⁶, Sathish Ganesan⁶, Shanmugham Venkatachalam Srinivasan⁶, Jutta Papenbrock⁵ and Dirk Weichgrebe¹

Abstract

The increase in mineral and ash-rich waste biomass (MWB) generation in emerging economies poses critical environmental problems and bottlenecks the solid waste and wastewater treatment systems. Transforming these MWB such as sewage sludge from wastewater treatment (SSW) to biochar can be a sustainable method for their disposal and resource recovery. However, such biochar has limited applicability due to the relatively low organic content and possibly contaminated nature of SSW. This may be offset through combined pyrolysis with other MWB, which can also support municipal solid waste management. Studies on this MWB co-pyrolysis are lacking and have not yet seen successful long-term implementation. This work is the second part of authors' research encompassing an analytical and lab-scale investigation of biochar production from MWB through pyrolysis for the case of Chennai city, India. Here, the physicochemical properties of biochar derived from lab-scale co-pyrolysis of SSW with other MWB such as anaerobic digestate from waste to energy plants of food, kitchen or market waste fermentation, and banana peduncles (BP) collected from vegetable markets and their thermolysis mechanism are comprehensively investigated for purpose of carbon sequestration. Also, a novel preliminary investigation of the effect of sample weight (scaling effect) on the analytical pyrolysis of biomass (BP as model substrate) is undertaken to elucidate its impact on the heat of pyrolysis and carbon distribution in resultant biochar. The maximum carbon sequestration potential of the derived biochar types is 0.22 kg CO₂ kg⁻¹ biomass. The co-pyrolysis of MWB is exothermic and governed by the synergetic effects of the components in blends with emission profiles following the order CO₂ > CH₄ > CO > NH₃. Co-pyrolysis reduced the heavy metal enrichment in SSW biochar. The derived biochars can be an immediate source of N, P and S in nutrient-deficient acidic soils. The biochar has only up to 4-ring polyaromatic compounds and a residence time longer than 1 h at 500 °C is necessary to improve carbonization. The heat released during analytical pyrolysis of the model biomass and distribution of carbon in the resultant biochar are significantly influenced by scaling effects, drawing attention to the need for a more detailed scaling investigation of biomass pyrolysis.

Keywords Waste management, Mineral and ash-rich biomass, Co-pyrolysis, Biochar, Carbon sequestration

*Correspondence:

Rahul Ramesh Nair

nair@isah.uni-hannover.de; rahulgenesis@hotmail.com

Full list of author information is available at the end of the article



© The Author(s) 2023. **Open Access** This article is licensed under a Creative Commons Attribution 4.0 International License, which permits use, sharing, adaptation, distribution and reproduction in any medium or format, as long as you give appropriate credit to the original author(s) and the source, provide a link to the Creative Commons licence, and indicate if changes were made. The images or other third party material in this article are included in the article's Creative Commons licence, unless indicated otherwise in a credit line to the material. If material is not included in the article's Creative Commons licence and your intended use is not permitted by statutory regulation or exceeds the permitted use, you will need to obtain permission directly from the copyright holder. To view a copy of this licence, visit <http://creativecommons.org/licenses/by/4.0/>.

1 Introduction

Rampant urbanization and resource utilization in emerging economies increase the generation of mineral and ash-rich waste biomass (MWB) such as sewage sludge, anaerobic digestate, and refuse lignocellulosic biomasses, which constrains the solid waste treatment (SWT) infrastructure in their urban areas. Global adoption of the waste hierarchy principle (prevention, reuse, recycling, and recovery) is essential to meet the UN sustainable development goal (SDG) 12.5 – “substantial reduction of waste generation by 2030” [1]. The integration of recycling and energy recovery from waste biomass into the national development strategies of these nations can aid in sustainable growth via a circular economy (CE). Industrialized countries have already made strides to achieve a CE. An example is the CE action plan adopted by the European Union in 2015 [2]. In such a CE development model, it is also necessary to sustainably upcycle the recycled products derived from SWT for utilization as secondary raw materials. Biomass can be valorized as biochar (carbonaceous residue) through slow pyrolysis in an inert or oxygen-deficient environment. This upcycling pathway converts waste biomass into a value-added product with multifaceted environmental applications such as carbon sequestration (UN SDG 13.2), soil amelioration (UN SDG 15.3), and adsorption of pollutants in water (UN SDG 6.3) [3]. Thus, the conversion of MWB into biochar has the potential to support SWT infrastructure in emerging economies while simultaneously tackling these four areas of the 2030 UN sustainable development agenda.

Despite the aforementioned benefits, biochar generation systems are still not widely implemented. The pyrolysis of biomass, particularly MWB, is a complex thermo-chemical process due to the interaction of various alkali and alkaline earth metals (AAEM), transition metal compounds, and other inorganics (e.g., silicates) with the lignocellulosic constituents. The inherent heterogeneity in MWB restricts the generalized modelling of their thermolysis mechanism. Sewage sludge from wastewater treatment (SSW) is an MWB that causes major bottlenecks in municipal wastewater treatment (WWT) in emerging economies. For instance, India produces ~ 3.95 Mt of dry SSW from only 32% of wastewater that is treated before disposal [4]. The commonly utilized SWT methods continue to be open-dumping and land-filling [5], which are also restrained by rising land costs, consumption and pollution trends. Recent attempts at waste-to-energy techniques for such MWB have also incurred significant failures [6]. Hence, there is an urgent need to investigate and design SSW treatment systems in this region that can also aid to mitigate climate change and support nutrient recovery in line with CE principles

[7]. Pyrolytic conversion of SSW into biochar can be one such treatment method. Owing to the heterogeneous nature of SSW (even comparing two cities within the same country) and the known constraints [8] associated with SSW pyrolysis, the thermolysis and resultant biochar properties must be analyzed on a case-by-case basis to evaluate their commercial viability.

Co-pyrolyzing SSW with other organic matter can render the SWT of such MWB economically viable [9] and may also improve the quality (soil applicability) of biochar derived from SSW [10, 11]. It is generally advised to mix SSW with other additives/materials to overcome the drawbacks of its pyrolysis. Though co-pyrolysis studies of SSW with agricultural residues are reported in the literature [12, 13], reports on combined pyrolysis of SSW with other MWB are generally lacking. The pyrolytic conversion of SSW is still considered technologically immature with reported implementation failure even in industrialized nations such as Germany [14]. A detailed investigation from the analytical to industrial scale becomes crucial in implementing biochar production from SSW. In the part-1 study [15], for the case of the southern Indian city of Chennai, the authors have investigated the analytical pyrolysis of three types of MWB that are a) rich in ash – digested SSW from a wastewater treatment plant (M100), b) rich in minerals – banana peduncle with high potassium concentration (M010), and c) rich in ash and minerals – anaerobic digestate from a food waste processing facility (M001).

In this part-2 study, biochar is produced through the co-pyrolysis of different blends of M100 with M010 and M001 in a lab-scale reactor and the physicochemical properties are comprehensively investigated and compared concerning their carbon sequestration potential. The thermal degradation mechanism during co-pyrolysis is analyzed through simultaneous thermal analysis (TGA–DSC) coupled with infrared spectroscopy (FT-IR). Then, for the first time, a preliminary investigation is carried out to evaluate the influence of the sample weight (scaling effect) during analytical pyrolysis of biomass since the heat and mass transfer effects can affect the thermolysis mechanism [16, 17] during analytical pyrolysis, which is generally used to model industrial and lab-scale processes.

2 Materials and methods

2.1 Materials

The MWB in this study was collected from Chennai, India. These included a) anaerobic digestate from an organic waste treatment facility collected by Central Leather Research Institute, Chennai (M001). b) banana peduncles (M010) from the Koyambedu vegetable and flower market, and c) anaerobically digested sewage

sludge (M100) from the Perungudi wastewater treatment plant. These constituted the unmixed baseline materials (BM) whose pyrolysis kinetics was investigated in the part-1 study [15]. Then, they were oven dried (105 °C for 48 h) and shredded to 0.2 mm particle size distribution. The elemental and proximate analysis of BM is shown in Table S1 of [supplementary materials](#) (SM). Seven blends of these three materials were prepared by keeping M100 at 50 wt% and varying the others. Table 1 shows the proportion of these MM, the labelling of different MM blends and the resulting biochar.

2.2 Lab-scale slow pyrolysis

About 25 g of each B-BM and B-MM were pyrolyzed in a lab-scale furnace (Fig. S1 of SM) by linear heating (10 °C min⁻¹) from 30 to 500 °C in 0.4–0.5 L min⁻¹ nitrogen flow. At the highest treatment temperature (HTT) of 500 °C, they were kept isothermal for 60 min. During this isothermal regime, the maximum temperature attained by the materials was termed the highest pyrolysis temperature (HPT). The biochar was recovered and stored in sealed containers for transport and analysis. The name of these biochar types includes the prefix 'B' as shown in Table 1.

2.3 Biochar characterization

The elemental analyses of C, H, N, and O were carried out by Mikroanalytisches Laboratorium Kolbe GmbH (Fürth, Germany) after overnight drying at 105 °C. In short, biochar samples were weighed and dried overnight at 105 °C. The elements C, H, S, and N were measured in the Mikro Cube CHNS analyzer (Elementar, Frankfurt, Germany). Oxygen was measured in Vario EL Cube (Elementar). The heavy metals (HM), micro (K, Mg, Na and Ca) and macronutrients (P, S) concentration in the

biochar were analyzed by inductively coupled plasma optical emission spectrometry (ICP-OES) iCAP 6000 (Thermo Fisher Scientific Corporation, Waltham, Massachusetts, USA). Infrared spectra (4000–400 cm⁻¹) of the biochar were collected using the method of Attenuated Total Reflection (ATR) using Nicolet iS50 (Thermo Fisher Scientific Corporation) having a KBr beam splitter, diamond crystal, and deuterated triglycine sulfate detector. The measurement parameters of optical velocity, signal gain, and aperture size were 0.1581 cm s⁻¹, 2.0, and 87, respectively. The FT-IR spectra were baseline-corrected. The aromatic to aliphatic ratio (A_i) was calculated according to the Eq. (1) where the region 1620–1530 cm⁻¹ represents the $\nu_{C=C}$ of the aromatic ring, and 1460–1270 cm⁻¹ includes δ_{as} CH₂, CH₃ and δ_s CH₃ of aliphatic structures [18].

$$A_i = \frac{\text{Area}_{1620-1530}}{\text{Area}_{1460-1270}} \quad (1)$$

Scanning electron micrographs were captured (12 kV and 15 kV, resolution 4) using Quanta 200 (FEI, Oregon, USA) after degassing in N₂ (for 6 to 8 min) and gold coating (at 25 mA for 2 min) the samples in Edwards S150A sputter coater. The vacuum condition for the electron gun was kept below 8.7 × 10⁻⁶ kPa. Nitrogen physisorption measurements were made at 77 K in NOVA 4000 (Quantachrome Instruments, Boynton Beach, FL) to calculate the pore surface area (S_{BET}) through Brunauer–Emmett–Teller (BET) method [19]. Before analysis, each biochar sample was vacuum degassed at 40 °C until the cell pressure approached nearly zero kPa. The thermal oxidative stability of biochar was analyzed using TGA/DSC 3 + /LF (Mettler Toledo, Ohio, USA). For this, 5 mg of each sample was combusted in 70 μ L alumina crucibles from 25 to 1050 °C under a synthetic air (purity of 99.999% from

Table 1 List of substrates – mixed and baseline materials – used for co-pyrolysis, and the names of the biochar derived from these materials

Name of biomass	Collective name of biomass	Proportion (in dry wt%)			Name of biochar	Collective name of biochar
		Sewage sludge	Banana peduncles	Anaerobic digestate		
M333	Mixed materials (MM)	33.3	33.3	33.3	B333	B-MM
M505		50	0	50	B505	
M514		50	10	40	B514	
M523		50	20	30	B523	
M532		50	30	20	B532	
M541		50	40	10	B541	
M550		50	50	0	B550	
M001	Baseline materials (BM)	0	0	100	B001	B-BM
M010		0	100	0	B010	
M100		100	0	0	B100	

Linde Gases GmbH) flow of 70 mL min⁻¹ and a heating rate of 10 °C min⁻¹. Then the thermal stability was evaluated as thermal oxidative recalcitrance (TOR_i) as defined in ref [20] using MATLAB R2020b. M010 is the only naturogenic feedstock among the materials. Hence it was used as the reference for evaluating the TOR_i. The volatile matter (VM), ash content and fixed carbon (FC) (collectively referred to as proximate analysis) were also measured using TGA. At first, samples were pre-purged in an N₂ flow of 40 mL min⁻¹ for 10 min. Residual moisture was removed isothermally at 110 °C for 10 min in an N₂ atmosphere. Then, it was linearly heated (50 °C min⁻¹ with 40 mL min⁻¹ N₂ flow) and kept isothermal at 950 °C for 10 min for the removal of VM. The sample was cooled to 550 °C and kept isothermal for 10 min in synthetic air (100 mL min⁻¹) to evaluate the loss-on-ignition. Finally, the sample was cooled to 110 °C in N₂ flow (40 mL min⁻¹) and kept isothermal for ash content determination. Measurements were made in triplicates and averaged. The total organic carbon (TOC) was measured in vario TOC cube (Elementar) after ~10 mg of biochar was treated with 1 M HCl to remove inorganic carbonates. The zeta potential (ζ) was analyzed using ZetaPALS (BrookHaven Instruments Corporation, New York, USA) with 5 runs (10 cycles per run) for each biochar.

The pyrolysis–gas chromatography–mass spectroscopy (Py-GC–MS) was performed in a double shot Pyrolyzer EGA/PY-3030D (Frontier Laboratories Ltd., Fukushima, Japan) connected to a Trace 1310 GC and ISQ 7000 Single quadrupole MS-System (Thermo Fisher Scientific). Unaltered ground samples (~25 mg) were placed in small crucibles and introduced into the furnace via autosampler (AS-1020E, F-Lab). The flash pyrolysis was performed at 800 °C and evolved gases were then directly injected into the GC/MS system for analysis. The gas chromatograph was equipped with a low-to-mid polarity Ultra Alloy[®] capillary column (UA⁺-5, F-Lab.) of 30 m × 250 μm × 0.25 μm film thickness. The carrier gas was helium at 1 mL min⁻¹. In the mass spectrometer, Total Ion Current chromatograms (TIC) were acquired at 70 eV ionizing energy. The acquired chromatograms were analyzed using GC–MS Postrun Analysis v4.52 (Shimadzu, Kyoto, Japan). Each chromatogram was processed with a background spectrum between 18 and 24 min and a smoothing window of 0.05 s. For peak detection and integration, a slope of 5000 min⁻¹ and a minimum height of 20 × 10⁶ units were used. The peaks were identified using the NIST database (search depth = 3, with reverse search enabled and minimum similarity index > 90).

The properties of water extractable fractions (WEF) such as pH, electrical conductivity (EC), and dissolved organic matter (DOM) were analyzed after extraction using a 0.45 μm syringe filter (CHROMAFIL[®] Xtra

Hydrophilic PES membrane). In short, ~100 mg of biochar was mixed with 10 mL of ultrapure water. Then, the solution was stirred (150 to 200 rpm) for 3 h using a magnetic stirrer. After stirring, the solutions were stored in a dark container for 24 h. Then, the suspension was filtered (0.45 μm), and the pH and EC of the supernatant were measured with a multimeter WTW MultiLine[®] Multi 3630 IDS SET F/ SenTix[®] 940/ TetraCon[®] 925/ FDO[®] 925. Dissolved organic carbon (DOC) was measured as non-purgeable organic carbon using Vario TOC cube (Elementar) with a measurement uncertainty of 2%. The UV–VIS spectra of supernatant in single-use cuvettes (layer thickness, l = 10 mm) were collected between 200 and 900 nm using DR6000 UV–VIS spectrophotometer (Hach, Colorado, USA). SUVA₂₅₄ (an indicator of DOM aromaticity) and E2/E3 (ratio of UV absorbance at 254 to 365 nm is inversely proportional to molecular weight of DOM) were evaluated. About 10 mL of this supernatant was used to measure the cations (K⁺, Na⁺, Mg²⁺, Ca²⁺, and NH₄⁺) and anions (Cl⁻, SO₄²⁻) in an Ion chromatograph (Thermo Scientific Dionex Aquion/Dionex Integron HPIC with Dionex AS-AP autosampler).

2.4 Pyrolysis characteristics

The pyrolysis of each MM (Table 1) was investigated using a TGA/DSC 3+LF thermal analyzer (Mettler Toledo) at six heating rates – (5, 7, 10, 12, 15 and 20 °C min⁻¹) between 25 and 1000 °C using 70 μL alumina crucibles (N₂ flow of 70 mL min⁻¹). Each measurement was preceded by a 10 min pre-purge using 100 mL min⁻¹ of N₂ and was performed in duplicates. The thermograms – weight loss/thermogravimetry (TG) curves, rate of weight loss or differential thermogravimetry (DTG) curves, reaction progress/conversions α (evaluated as in Eq. (2)) and heat flow per unit weight – were plotted against reference temperature and time.

$$\alpha = \frac{\text{initial sample mass} - \text{instantaneous sample mass}}{\text{initial sample mass} - \text{final sample mass}} \quad (2)$$

During the thermal analysis, the condition of linearity of heating rate (minimal difference between sample and reference temperature) is satisfied. For the calculation of heat of pyrolysis (HoP) at 15 °C min⁻¹, DSC readings were blank corrected against an empty crucible and normalized by sample weight. They were then subtracted with a spline baseline since DSC readings of such heterogeneous material would also be influenced by its specific heat capacity which tends to change with temperature. The HoP at any required region was calculated by the integration of this DSC curve (W g⁻¹) against time (s). A Nicolet iS50 FT-IR (Thermo Fisher Scientific) was used (resolution, optical velocity, aperture, and signal gain of

8 cm⁻¹, 0.4747 cm s⁻¹, 100, and 1.0, respectively) for tracing the evolved gas profiles of CO₂ (2400–2250 cm⁻¹), CO (2250–2000 cm⁻¹), CH₄ (3020–2800 cm⁻¹) and NH₃ (980–920 cm⁻¹) during the pyrolysis.

2.5 Scaling effect

A preliminary investigation of the scaling effect was carried out for the case of M010. After a 100 mL min⁻¹ flush with N₂ for 10 min, 12 sample sizes of M010 were linearly heated (20 °C min⁻¹ with 80 mL min⁻¹ N₂ flow) in 900 µL alumina crucibles from 25 to 650 °C. Twelve sample sizes from 5 to 500 mg (labelled as scl_5, scl_500 etc.) were used. Duplicate to triplicate trials was performed for each sample (more trials for sizes less than 25 mg) and averaged to plot the thermograms. Each crucible used in each trial was blank-corrected with the same heating program to minimize errors and DSC baseline drifts. The HoP was evaluated as mentioned earlier. The biochar produced at these different scales was then investigated for aromatic carbon content and total carbon (TC). TC was measured in the vario TOC cube (Elementar) through the combustion of 6 to 15 mg of biochar sample at 950 °C. Glutamine was used as the reference standard. Duplicate to triplicate measurements were made, depending on biochar availability. The ¹³C solid-state NMR (ssNMR) cross-polarization (CP) and direct polarization (DP) experiments are performed on a 600 MHz SB Bruker Avance III spectrometer (Bruker, Billerica, MA, USA) equipped with commercial 3.2 mm magic angle spinning (MAS) E-free ¹H,¹³C,¹⁵N probe head. Typically, around 30 mg of biochar was packed into a thin wall ssNMR rotor. All experiments are carried out at 16 kHz MAS rate and temperature of 275 K. Typical ¹H and ¹³C 90° pulse lengths were 3.5 µs and 5.0 µs, respectively; the length of CP contact time was 2 ms. A SPINAL64 decoupling [21] of 70 kHz field strength was applied during acquisition. In total, 32,768 scans with 2 s recycle delay were acquired for each CP spectrum. In total, 2048 scans with 15 s recycle delay was acquired for each DP spectrum. The CP and DP spectra were baseline corrected and normalized to the sample mass for further semi-quantitative analysis. The chemical shifts of aryl C, alkyl C and carbonyl C were assigned 110–165 ppm, 50–110 ppm, and 165–200 ppm, respectively. A relative spin counting for the relative NMR-observable carbon (RC) at the different mass scales was calculated according to Eq. (3), where I* is the normalized total integral between 50 and 200 ppm, and TC is the total carbon content.

$$RC = \frac{I^*}{\text{sample mass} \times TC} \quad (3)$$

Though total suppression of sidebands was not performed for CP MAS acquisition, the method of

mathematical spinning sideband (SSB) subtraction was avoided because it could underestimate the intensities of SSBs arising from aromatic moieties and those from the hidden ones [22].

2.6 Statistics

The descriptive statistics of the analyses were calculated in OriginPro 2021, while statistical tests were performed using IBM SPSS v28.0. For elemental analysis, the measurement uncertainty was ±0.01% for C, H, and N, and ±0.015 for S. The mean std deviation of S_{BET} and ζ potential for the biochars was ±0.419 m² g⁻¹ and ±3.747 mV, respectively. The weight and heat flow data during the TGA/DSC trials were reproducible with the std deviations lying within an acceptable range. For instance, the mean and standard deviation of the thermograms of the mass-scaling experimental runs of M010 is shown in Fig. S2 of SM.

3 Results & discussion

3.1 Biochar yield and pyrolysis process

The biochar yield (wt%) and HPT (°C) of BM and MM during the lab-scale pyrolysis are shown in Fig. 1. Among the BM, the yield and the HPT during the process are proportional to their ash content – M100 > M001 > M010. Inorganics are a significant portion of MWB such as M100 and M001. For the MM, the yield of M505 is the highest while that of M523 is the lowest. The yield has no significant correlation (R²=0.171) with the proportions of M010 and M001 blended with M100. This may be because the pyrolysis of such blended biomass is influenced more by synergetic effects amongst the different blend constituents as seen in refs [23, 24].

3.2 Biochar properties

The elemental analyses – C, H, N, and O – of biochar are shown in Table 2. The molar ratios are calculated based on the total organic carbon (C_{org}) to avoid interference from inorganic carbonates inherited from M001 and M100. Biochars derived at temperatures above 400 °C can have aromatic clusters. The molar ratio of H/C_{org} is correlated to an n*n aromatic cluster size for H/C_{org} ≤ 1 as in ref [25] (Eq. (4)). B514 and B550 can have large aromatic clusters up to 3*3 while others, except B001, may have up to 2*2. Thus, these biochars do not contain high molecular weight aromatic compounds. This may be because the HTT and residence time is insufficient to cause extensive polycondensation [26]. Hence, their porosity can also be low.

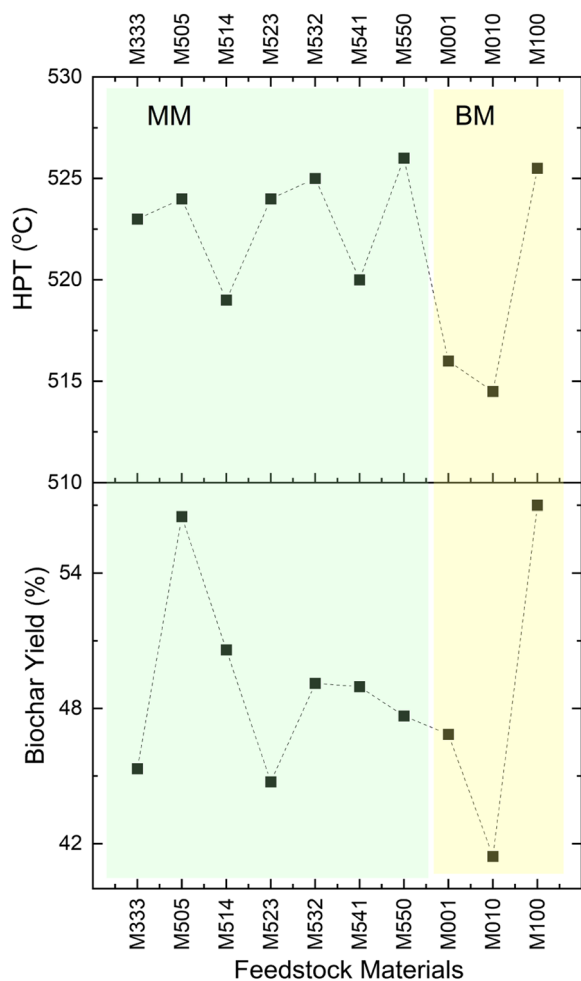


Fig. 1 The biochar yield and highest pyrolysis temperature (HPT) reached by the feedstock materials (MM and BM) during their lab-scale pyrolysis

Table 2 Elemental analyses (in dry wt% of biochar prepared through lab-scale pyrolysis of BM and MM at 500 °C

Biochar	C Dry wt%	H	N	O
B333	32.64	1.49	1.88	14.79
B505	17.99	1.07	1.68	15.07
B514	17.39	0.93	1.45	14.62
B523	19.79	1.20	1.61	12.34
B532	24.20	1.24	2.10	14.31
B541	25.14	1.63	1.34	16.73
B550	21.03	1.07	1.90	14.81
B001	21.83	2.27	1.15	16.74
B010	41.89	3.21	1.20	21.14
B100	9.48	0.56	0.43	9.17

$$\frac{H}{C_{org}} = \frac{2 + 4n}{2n^2 + 4n} \tag{4}$$

Table 3 shows the proximate analysis results (moisture, ash, VM and FC), ash-free biochar yield and TOR_i for B-BM and B-MM. Along with water, mass loss below 120 °C during the proximate analysis can also include adsorbed alcohols and low molecular weight tar released during pyrolysis. It can be seen that a) B550 and B010 have the highest (VM) due to the insufficient carbonization of holocellulose, b) B-MM have high ash content compared to biochar from lignin-rich feedstock like wood and walnut shells, and c) VM increased with the introduction of less-polymerized organic waste (M010) during co-pyrolysis. Ash in B-MM is mainly derived from M100 (Table S1 of SM) and co-pyrolysis helps in reducing this problem. The biochars B333, B505 and B514 exhibit a ~23% increase in (FC) relative to their respective parent biomasses, while others register a decrease. This is because FC in biochar with ash >20% is poorly correlated with that of their parent biomass due to the influence of inorganics during pyrolysis, and interference of ash in the estimation of FC [27]. The ash-free yield of all B-MM is ~20 dry wt%. B100 is the most stable (TOR_i=0.41) owing to its highest ash while B333 is least stable with TOR_i=-0.15 (despite having similar VM relative to other B-MM) which may be from the synergetic effects of its minerals and ash during the thermal oxidation process. The stability (mass loss during thermal oxidation) of the biochars is significantly (*p*<0.05) correlated to total carbon (Pearson $\rho = 0.847$) and ash ($\rho = -0.823$).

For such mineral and ash-rich biochar (MAB), a conventional van Krevelen diagram is error-prone (since the determination of oxygen requires ash correction which is not reliable [28]) and a plot of H/C vs Ash/C is recommended [29]. Figure 2 shows the plot of H/C vs Ash/C and the van Krevelen diagram for B-MM and B-BM. Here, B333, B532, B550 and B514 fall under the definition of MAB. Literature suggests that pyrolysis temperatures between 350 to 500 °C are sufficient for the carbonization of biomass through slow pyrolysis [26]. Here, even the cellulose-rich M010 (H/C_{org}=1.09) has not been sufficiently transformed, implying that the residence time is the limiting factor. Furthermore, except for B541 and B505, co-pyrolysis has generally increased the carbonization (H/C_{org}) relative to B100 as seen in the case of sludge and wetland biomass waste [30].

Due to high ash, the O/C_{org} does not have a statistically significant correlation with VM (R²=0.349 and *p*=0.072). Similarly, there is no correlation between H/C_{org} and VM. The consensus that measured VM represents the labile C, -O and -N functional groups in biochar [31] is not always valid when the pyrolysis HTT is

Table 3 Proximate analyses results (water content, ash, VM, and FC), ash-free biochar yield, thermal oxidative recalcitrance (TOR_i), pore surface area (S_{BET}) and zeta (ζ) potential of B-BM and B-MM

Biochar	Moisture Dry wt%	Ash	Volatile matter (VM)	Fixed carbon (FC)	Ash-free yield	TOR_i	S_{BET} $m^2 g^{-1}$	ζ potential mV
B333	5.39	50.81	28.32	20.87	23.53	-0.15	4.42	-31.16
B505	2.49	61.72	29.51	8.77	22.5	0.26	8.09	-27.06
B514	3.73	62.41	25.17	12.42	20.2	0.18	6.02	-38.64
B523	3.74	62.88	25.71	11.4	17.66	0.21	6.08	-34.17
B532	3.87	60.48	26.46	13.05	20.56	0.13	7.59	-47.35
B541	3.29	60.11	29.75	10.14	20.51	0.20	5.42	-41.61
B550	3.63	58.32	33.76	7.92	20.87	0.21	5.36	-48.50
B001	1.57	73.31	17.35	9.34	13.04	0.25	4.71	-31.86
B010	5.21	38.76	33.58	27.66	26.21	0.00	6.39	-48.89
B100	0.84	84.27	15.5	0.23	9.37	0.41	4.63	-25.06

low compared to the temperature at which VM is measured because a) carbonates and some polyaromatics can also decompose [32] during the measurement of VM and b) variability in measurement techniques [33]. Thus, VM is not completely representative of the labile fraction in MAB. As per International Biochar Initiative (IBI) standards [34], based on H/C_{org} , the most carbonized biochar types here are B550 and B514, and they belong to class 2 ($10\% \leq C_{org} \leq 30\%$). At least 50% of their carbon will be stable in soil for 100 years (BC_{+100}). The carbon sequestration potential of B550 and B514 (calculated as per ref [35]) are 0.21 and 0.22 $kg_{CO_2} kg_{biomass}^{-1}$ respectively. They can mitigate the N_2O emissions from the soil by $\sim 40 \pm 16\%$ [36]. Despite having a similar VM, B550 is more carbonized compared to B010 at 500 °C due to the synergetic influences during co-pyrolysis. This further confirms that proximate analysis cannot be used to predict the stability of MAB.

The pores in these MAB are not well developed with $S_{BET} < 10 m^2 g^{-1}$ (Table 3) due to large ash concentrations, tar clogging the pores (also seen in the literature [37, 38]) and inadequate carbonization as seen above. B505 has the highest S_{BET} of only $8.1 m^2 g^{-1}$, which tends to decrease with the ratio of M010 to M001 in the MM. This can be either from the coking of volatiles introduced by M010 that subsequently block pores [39] or from the volatiles that has not sufficiently carbonized and then occupies the porous network of minerals present in M100 and M001. Except for B505 and B100, others are colloiddally stable ($\zeta < -30$ mV). The negative surface charge of these biochar types stems from the acidic oxygenated functional groups from the uncarbonized organics that deprotonate in water. The molar ratios O/C and (N+O)/C should not be correlated with hydrophobicity and polarity index, respectively, as seen in ref [40] since most O is bonded

in the form of silicates in ash and inorganic carbonates. Figure S3 (SM) shows the IR spectra of B-BM and B-MM and their calculated A_i . The peak regions $1470-1430 cm^{-1}$, and $3600-3000 cm^{-1}$ are from functional groups of O – CH_3 , and –OH, respectively. The low A_i of B100 is due to its low C_{org} , while that of B010 is due to a lack of carbonization. The A_i does not follow the trend of H/C_{org} ratios of biochars. This is because the surface measurement nature of the ATR technique may not reveal the complete A_i in MWB biochars. However, it can be confirmed that, unlike in ref [41], co-pyrolysis of sludge has increased the aliphatic functional groups present in biochar. This is because, as in the aforementioned ref, up to 2 h of residence time may be required for sludge co-pyrolysis in this reactor.

Table S2 in SM shows the heavy metal, micronutrients (K, Mg, Na and Ca) and macronutrient (P, S) content ($mg g^{-1}$) in the biochar measured by ICP-OES. The synergy during co-pyrolysis influences the concentration of these elements (Fig. S4 of SM). M001 and M010 were able to reduce the Pb and Cu enrichment in M100, which is a major constraint in the application of sludge biochar [42]. This effect is usually attributed to the dilution effect that occurs during co-pyrolysis [39]. However, the Cu in B-MM is still higher than the land application limit of $0.10 mg g^{-1}$. The enrichment of Cr, Ni, and Zn in B-MM are also above their limiting values of 0.09, 0.03, and $0.40 mg g^{-1}$, respectively, as specified by the European Biochar Certificate [43]. Hence, B-MM is not suitable for direct land application, unless mixed with other soil ameliorators such as compost or organic fertilizers. However, despite the net HM enrichment, such biochar can have low exchangeable (acid soluble and carbonate bound) and a reducible fraction (bound to Fe and Mn oxides) – the most bioavailable forms of HMs. The exchangeable

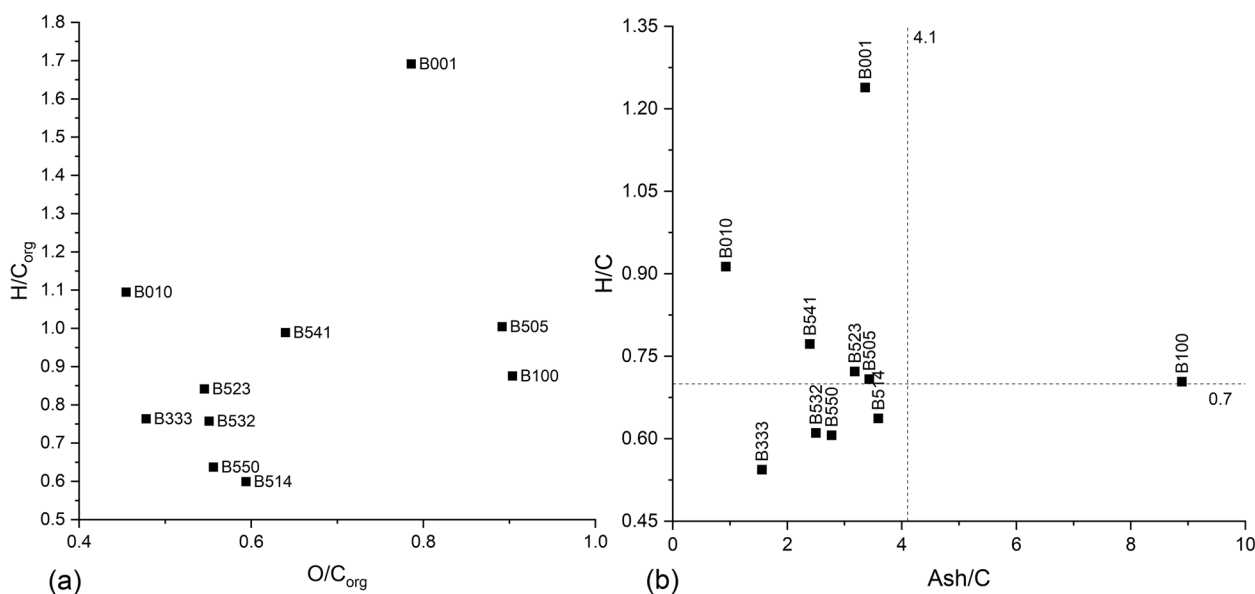


Fig. 2 A van Krevelen diagram (b) of the biochar types under study; and plot of H/C vs Ash/C (a) showing mineral and ash-rich biochar (MAB) defined by $H/C \leq 0.7$ and $Ash/C \leq 4.1$

fraction of HMs can further transform into less bioavailable forms with increasing residence time. On the other hand, B-MM has higher concentrations of P and S which are essential plant nutrients. It is not recommended to increase the HTT to improve the carbonization of BM since it would concurrently raise the HM enrichment and pH. But, for biochars produced at HTTs around 500 °C, increasing the residence time may be another option to improve carbonization [44] and provide sufficient energy for the transformation of the acid exchangeable fraction of HMs to less bio-available forms.

During the analytical pyrolysis, the evolved products from the three B-MM are listed in Table 4. Since the biomass was pyrolyzed at 500 °C HTT, the evolved compounds during analytical pyrolysis at 800 °C also include the new pyrolysis products formed from any remaining uncarbonized biomass fraction. Peak tailing and double peaks were seen for some evolved compounds due to the large sample mass and the release of trapped volatiles from pores and the surface of biochar. The initial broad peaks are attributed to CO_2 . Methoxylated monophenols and cresols are common products of lignin pyrolysis. Key markers of cellulose are levoglucosan ($C_6H_{10}O_5$) and 1,4:3,6-dianhydro- α -D-glucopyranose, while that of hemicellulose are ketones such as acetone and 1-hydroxy-2-butanone. The absence of these markers indicates negligible holocellulose remnants in B010 [45]. The absence of furans (mainly formed during holocellulose pyrolysis) also confirms this inference [46]. Long-chained aliphatic hydrocarbons (LAH) such as eicosane,

dodecane, pentadecane and 1-heptadecene and recalcitrant organic aromatic compounds such as indole are formed from chain length shortening of aliphatic C in biomass. They represent an intermediate stage before aromatic condensation (through hydrogen abstraction and carbon addition) and are commonly present in biochar prepared at HTT below 500 °C [47]. BTEX compounds such as benzene, toluene, ethylbenzene, and xylene are markers of pyrogenic carbon from carbohydrates [48] and are also formed during analytical pyrolysis itself through the demethoxylation and/or dehydrogenation of methoxy or phenolic compounds. Chromatogram peaks of pyridine and benzonitrile that are more prominent in B100 and B001 signify that nitrogen functionalities have not been eliminated during the devolatilization of BM. The relative prominence of polyaromatic hydrocarbons (PAH, e.g., fluorene, anthracene, fluoranthene, benz[a]anthracene) and alkyl-PAH over LAH are seen in B100 and B001. More N-compounds (such as quinoline, isoquinoline and carbazole) are also seen in B100 and B001. PAH in B010 and B100 is limited to 4-rings, while B001 also shows 5-ring compounds – perylene and benzo[j]fluoranthene. For B-MM, the evolved compounds constitute more LAH with an increasing contribution of M010 in the blends (Table S3 in SM) and aromatics are limited to a maximum of 4-ring benz[a]anthracene. This further confirms that with more residence time these LAH can be transformed further, thereby increasing the carbonization of B-MM. Another discernible difference is that nitrous oxide seems to evolve from biochar derived from

Table 4 List of identified compounds, their relative %-area, and similarity index during the analytical pyrolysis (using Py-GC–MS) of B-BM

Peak #	For the biochar B001			For the biochar B010			For the biochar B100		
	Area %	Similarity index	Compound	Area %	Similarity index	Compound	Area %	Similarity index	Compound
1	64.96	97	Carbon dioxide	68.62	97	Carbon dioxide	85.07	95	Carbon dioxide
2	16.38	97	Benzene	6.94	97	Benzene	1.00	98	o-Xylene
3	0.62	95	Cyclobutene, 2-propenylidene-	0.50	94	Phenol, 4-[2-(methylamino)ethyl]-	1.76	98	Styrene
4	4.31	96	Toluene	3.08	97	Toluene	1.30	95	Phenol
5	0.34	96	Ethylbenzene	1.58	95	Cyclobutene, 2-propenylidene-	1.12	98	Benzonitrile
6	0.65	98	o-Xylene	0.25	96	2-Acetyl-2-methyltetrahydrofuran	0.38	92	Azetidene, 3-methyl-3-phenyl-
7	1.45	98	Styrene	0.35	94	Pyridine, 3-methyl-	0.46	97	Benzene, 1-ethynyl-4-methyl-
8	0.79	95	Phenol	1.12	97	Ethylbenzene	2.27	99	Naphthalene
9	0.80	98	Benzonitrile	1.06	98	o-Xylene	0.23	97	Cyclopenta[c]thiapyran
10	0.26	94	Benzene, 1-ethenyl-4-methyl-	0.48	95	p-Xylene	0.53	98	Isoquinoline
11	0.32	91	Benzofuran	0.16	99	Nitrous Oxide	0.26	99	Quinoline
12	0.41	97	Benzene, 1-ethynyl-4-methyl-	0.31	91	1-Nonene	0.28	95	Indole
13	2.72	98	Naphthalene	1.30	98	Styrene	0.64	98	Naphthalene, 2-methyl-
14	0.32	98	Isoquinoline	0.51	94	Benzene, 1-ethyl-3-methyl-	0.43	98	Naphthalene, 1-methyl-
15	0.13	98	Quinoline	0.69	95	Phenol	0.55	98	Biphenyl
16	0.23	96	Indole	0.41	94	Benzoic acid, 2-fluoro-, 2-oxo-2-phenylethyl ester	0.14	95	Biphenyl
17	0.52	98	Naphthalene, 2-methyl-	0.80	93	Benzonitrile	0.31	97	Acenaphthylene
18	0.34	98	Naphthalene, 1-methyl-	0.67	93	Ethanone, 2-(formyloxy)-1-phenyl-	0.12	97	Naphtho[2,1-b]furan
19	0.46	97	Biphenyl	1.04	92	Indene	0.16	98	2-Naphthalenecarbonitrile
20	0.26	98	Acenaphthylene	2.87	92	m-Cresol	0.37	95	Dibenzofuran
21	0.29	96	Dibenzofuran	0.55	94	1H-Indene, 3-methyl-	0.35	96	Fluorene
22	0.25	95	Fluorene	0.26	94	1-Dodecene	0.12	97	Dibenzothiophene
23	0.86	98	Phenanthrene	0.35	96	Dodecane	0.75	98	Phenanthrene
24	0.18	96	9H-Fluorene, 9-methyl-	1.27	98	Azulene	0.29	98	9H-Carbazole, 9-nitroso-
25	0.22	98	9H-Carbazole, 9-nitroso-	0.13	90	1H-Indene, 1-ethylidene-	0.12	97	Phenanthrene, 2-methyl-
26	0.10	97	Anthracene, 1-methyl-	0.35	95	Tetradecane	0.17	98	2-Phenyl-naphthalene
27	0.17	97	2-Phenyl-naphthalene	0.46	95	Indole	0.22	97	Fluoranthene
28	0.33	97	Fluoranthene	0.58	97	Naphthalene, 2-methyl-	0.24	97	Pyrene
29	0.35	97	Pyrene	0.33	98	Naphthalene, 1-methyl-	0.11	97	7H-Benzo[c]fluorene
30	0.41	97	Benz[a]anthracene	0.78	96	Biphenyl	0.24	97	Benz[a]anthracene
31	0.36	97	Benzo[j]fluoranthene	0.21	97	Acenaphthylene			
32	0.21	96	Perylene	0.13	96	Pentadecane			

Table 4 (continued)

Peak #	For the biochar B001			For the biochar B010			For the biochar B100		
	Area %	Similarity index	Compound	Area %	Similarity index	Compound	Area %	Similarity index	Compound
33				0.36	96	Fluorene			
34				0.17	95	1-Heptadecene			
35				0.19	95	Tetatriacontane			
36				0.40	96	9H-Fluorene, 4-methyl-			
37				0.13	95	Eicosane			
38				0.16	95	Anthracene			
39				0.12	97	Fluoranthene			
40				0.17	96	Pyrene			
41				0.17	95	Benz[a]anthracene			

those blends where all BM were present – B514, B523, B532, B541 and B333.

The properties of WEF from the biochar are shown in Table 5. The EC and pH of WEF have a strong negative correlation ($\rho = -0.888$, $p < 0.01$ and $\rho = -0.791$, $p < 0.01$, respectively) with the ash content, and a strong positive correlation ($\rho = 0.933$, $p < 0.01$ and $\rho = 0.771$, $p < 0.01$, respectively) with VM in biochar, respectively, similar to that seen in refs [49, 50]. Usually, when prepared at high HTTs, EC of biochar tends to increase with higher ash content due to the dissolved ions from the ash fraction. However, when biochars have large VM content, the dissolved ions from the VM dictate the EC. Here, for instance, EC amongst the B-BM is influenced mainly by K^+ and Cl^- present in VM incorporated by M010. Except for B100, biochars are alkaline due to the carbonate and chloride forms of AAEM [50]. B100 is acidic due to the hydrolysis of Fe compounds present that releases H^+ ions [49]. B100 is also saline ($EC \approx 4 \text{ dS m}^{-1}$) due to the high concentrations of Cl^- and Na^+ ions that may induce salinization problems, if applied to agriculture in arid regions. Water extractable N, P, K, Mg, Ca, and S are nutrients directly available to plants in the short term. B-MM are rich in SO_4^{2-} and K^+ , while water-leachable $NO_3^- - N$ is low and below the quantification limit of the instrument. After devolatilization, the remaining N must be in aromatic C structures that are non-water leachable as seen during the analytical pyrolysis. The low water-available form of P is common among biochars [31] and arises from the immobilization of P as minerals by multivalent metal cations of Al, Mg, Ca, and Fe under alkaline pH. Though this P is not readily mobilizable it can become a long-term source, which does not get lost through surface runoffs. Ions of Ca and Mg are much lower in the WEF due to the relatively low solubility of their carbonates and oxides in water. Hence,

the B-MM and B-BM are not balanced commercial fertilizers [51]. The DOC from B010 is the highest since M010 has the most VM. However, $SUVA_{254}$ shows that this DOC mainly constitutes hydrophilic aliphatic compounds (since $SUVA_{254} < 3 \text{ L mg}^{-1} \text{ m}^{-1}$, except in B523, an outlier). N, P and S are important soil macronutrients and the maintenance of optimal carbon-nutrient ratios of C:N, C:P and C:S of biochar are essential for healthy soil microbial growth. These ratios of B-BM and B-MM compared with that of average soil [52] are shown in Fig. S5 (SM). Under the assumption of homeostasis and carbon-controlled microbial communities, B-MM tends to increase the carbon use efficiency of microbes as the nutrient ratios are at or below the soil limits. Thus, microbes can be energy limited and mobilize the excess N, P, and S, improving plant availability of these macronutrients in the short term due to low microbial demand. Hence, B-MM is suitable for addition in nutrient-deficient soil systems.

3.3 Co-pyrolysis characteristics

As the heating rate increases from 5 to $20 \text{ }^\circ\text{C min}^{-1}$, the rate of decomposition increases, and max peak decomposition shifts towards higher temperature in all reaction stages. This is because biomass is a poor conductor of heat and, even at small sample weights (1 to 10 mg), higher heating rates cause temperature gradients within the substrate owing to the ineffective heat transfer amongst the particles. The Figs. S6–S12 in SM show the thermograms – TG, DTG, conversions, and DSC curves – of all MM at six heating rates (5, 7, 10, 12, 15 and $20 \text{ }^\circ\text{C min}^{-1}$) between 25 and $1000 \text{ }^\circ\text{C}$. Furthermore, multiple reactions can concurrently initiate at higher heating rates (and cause higher degradation rates) thereby impeding the contact time of evolved volatiles with the substrate. This lowers the secondary char formation

Table 5 Properties of water extractable fraction (WEF) from the B-BM and B-MM derived from lab-scale pyrolysis

Parameters	Unit	B505	B514	B523	B532	B541	B550	B001	B010	B100
pH range		10.55 to 10.68	10.22 to 10.25	10.32 to 10.40	10.46 to 10.47	10.10 to 10.13	9.94 to 9.98	7.75 to 8.65	10.07 to 10.15	6.46 to 6.75
EC	dS m ⁻¹	2.74±0.04	1.87±0.02	2.08±0.07	2.19±0.03	2.34±0.04	3.8±0.04	0.69±0.07	3.97±0.1	0.47±0.05
Mean SUVA ₂₅₄	L mg ⁻¹ m ⁻¹	2.20	2.13	5.02	1.69	1.06	1.07	0.20	1.03	0.05
DOC	mg L ⁻¹	5.13±1.76	4.91±2.86	5.62±1.78	9.31±2.75	9.73±0.26	8.87±2.03	21.87±5.38	59.63±14.39	19.43±1.94
Cl ⁻		64.36±2.61	60.93±18.97	98.1±40.49	167.93±35.34	129.14±7.51	149.98±33.21	64.93±5.18	288.18±1.61	11.22±0.82
SO ₄ ²⁻		207.47±44.04	624.9±98.41	366.83±116.28	299.58±66.12	820.75±282.42	356.16±79.89	201.3±40.36	46.47±0.78	22.495±9.9
SO ₄ ²⁻ -S		69.25±14.7	208.57±32.85	122.44±38.81	99.99±22.07	273.94±94.26	118.87±26.66	67.19±13.47	15.51±0.26	75.08±3.3
Na ⁺		345.38±85.5	618.68±106.14	466.69±123.53	335.66±50	223.69±0.64	132.09±129.48	334.79±26.49	272.59±26.27	283.87±67.14
K ⁺		620.28±166.61	1052.57±180.26	617.71±187.68	583.53±133.57	2332.94±1055.29	1695.23±304	116.86±10.21	1504.72±7.09	13.76±3.2
Mg ²⁺		0.43±0.01	0.48±0.05	0.76±0.12	1.5±0.26	4.51±0.38	4.73±1.44	0±0	0±0	0±0
Ca ²⁺		4.06±0.11	9.16±0.53	6.26±0.08	14.37±0.61	26.12±0.38	21.73±7.23	0±0	0±0	84.76±6.12
PO ₄ ³⁻		0±0	1.75±2.47	4.55±0.48	0±0	0±0	10.46±2.19	0±0	0±0	0±0
PO ₄ ³⁻ -P		0±0	0.57±0.81	1.48±0.16	0±0	0±0	3.41±0.72	0±0	0±0	0±0

^aThose parameters with values of 0 are below the quantification limit of the instrument

reactions and reduces the char yield as seen in the TG curves of all MM. Such changes in char yield are more pronounced during high-temperature gasification in presence of various AAEM and ash constituents of MM, which also renders this region relatively endothermic. The biochar yields are statistically independent (Sect. 4.2 in SM) of heating rates except for M532 and M541 due to the sample heterogeneity induced by M001 and M100.

The thermograms of all MM at the heating rate of $15\text{ }^\circ\text{C min}^{-1}$ are shown in Fig. 3. By $500\text{ }^\circ\text{C}$ ~69–78% of the reaction is complete in all MM with a mean biochar yield of 52%. The identified pyrolysis reaction stages are (i) moisture removal $\leq 145\text{ }^\circ\text{C}$, (ii) organic matter decomposition – a combination of active pyrolysis and secondary heterogeneous reactions, (iii) decomposition of inorganic carbonates, and (iv) decomposition of other minerals and gasification above $\sim 830\text{ }^\circ\text{C}$. In all but M532, stage 1 has an additional peak at $\sim 130\text{ }^\circ\text{C}$ possibly from the removal of chemically bound water. Detailed information on these stages is in Table S4 and S5 (SM). The increasing proportion of M010 in the co-pyrolysis blends lowers the peak onset temperature of stage (ii) from 207

to $187\text{ }^\circ\text{C}$ due to the higher hemicellulose and catalytic effect of K as seen in another biomass thermolysis [53]. In this stage, the max peak decomposition temperature is delayed to $319\text{ }^\circ\text{C}$ for M505 due to low synergetic influence from M010 and the max peak decomposition rate increases with the ratio of M010 to M001 due to the increase in organics with M532 as an outlier.

From part-1 study [15] and Table S5, mixing M010 with M100 has shifted the active pyrolysis of sludge to lower temperatures, reduced the biochar yield and increased the exothermic heat release. An increase in temperature to $600\text{ }^\circ\text{C}$ makes the process more energy intensive. This is in contrast to co-pyrolysis of SSW with wheat straw [23] and SSW with wood powder [54] where the exothermicity occurs mainly after $700\text{ }^\circ\text{C}$ due to the late onset of secondary pyrolysis of char, which was also seen in the individual pyrolysis of M100 and M101 in the previous study. This difference depends on the temperature range at which the exothermic char condensation reactions takes place. When these reactions occur predominantly in the active pyrolysis regime, exothermic heat of pyrolysis is seen at lower

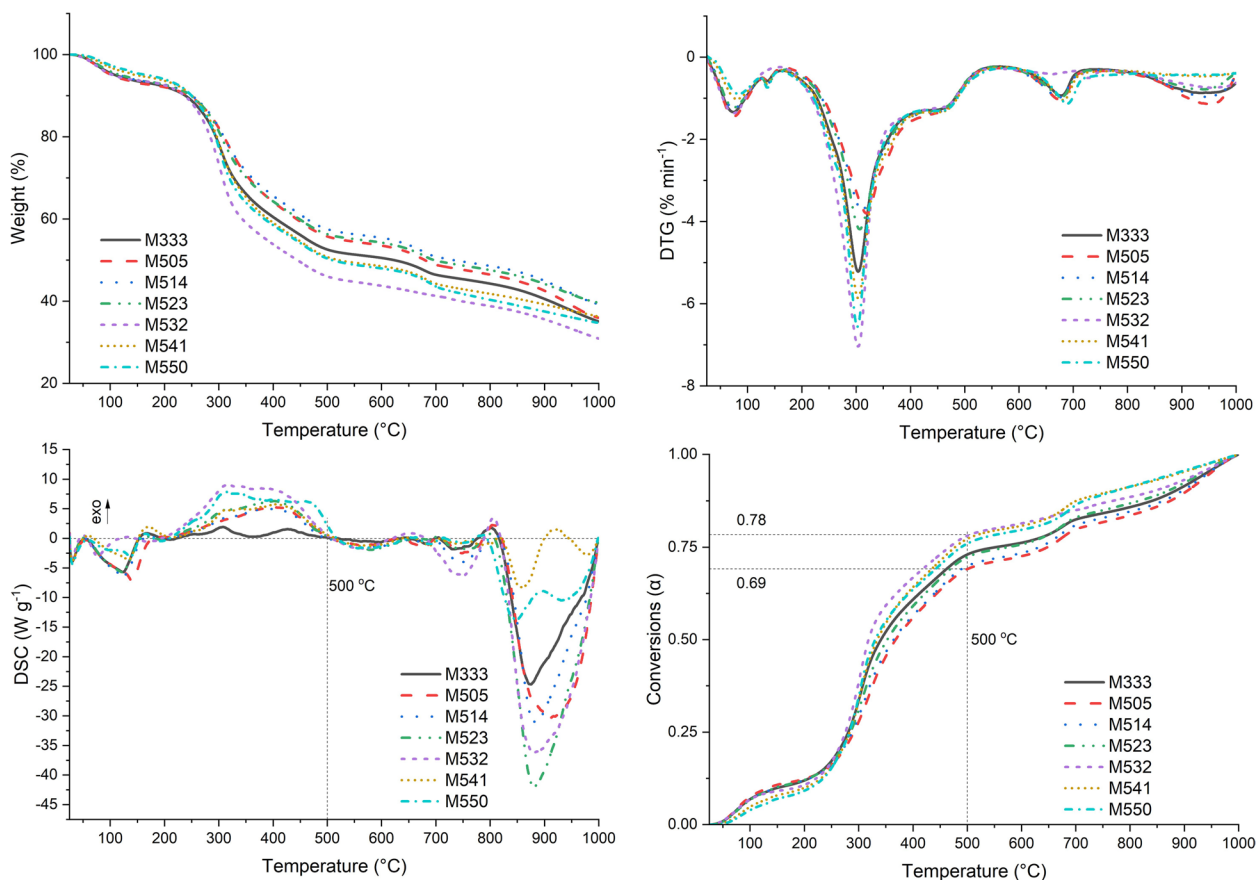


Fig. 3 The thermograms – TG, DTG, conversions, and DSC curves – during the pyrolysis of MM at $15\text{ }^\circ\text{C min}^{-1}$. In DSC, curves below 0 W g^{-1} denote endothermic heat flow

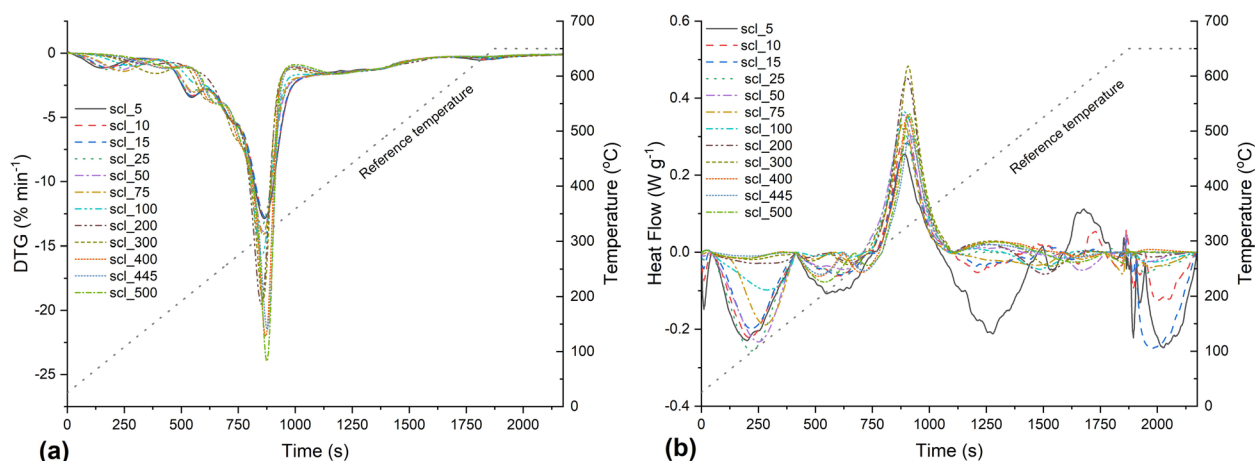


Fig. 4 Rate of mass loss (a) and heat flow curves (b) of M010 during pyrolysis at 20 °C min⁻¹ at different mass scales inside the TG reactor plotted against pyrolysis time. The legends scl-5, scl_10 etc., denote different mass scales inside TGA such as 5 mg, and 10 mg, respectively

temperatures as in co-pyrolysis of SSW with sugar cane bagasse [55] and with rice husk [56]. Here, this is another reason (in addition to HM enrichment) for limiting the pyrolysis of MM to 500 °C. Stages (iii) and (iv) are endothermic (DSC curve < 0) for all MM. However, between 700–900 °C, there is a small exothermic peak as in ref [23] due to interactions between the ash components and the biochar. This peak was absent in the pyrolysis of M100 [15]. The evaluation of deviations in weight loss (ΔW) between theoretical and experimental TG curves of the MM (Section S4.3 and Fig. S13 in SM) confirms the synergy between the components in the MM as seen in ref [13]. After stage 1, M505, M532, and M550 show a statistically significant (min std deviations) catalytic synergy during pyrolysis.

The relative emission intensities during active pyrolysis follow the order $\text{CO}_2 > \text{CH}_4 > \text{CO} > \text{NH}_3$ (Fig. S14 of SM). Here, CO_2 mainly evolves from the fracture of carboxyl and carbonyl groups of holocellulose. Therefore, M505 and M514, with their low holocellulose content, have the smallest CO_2 peaks. For M550, M541, and M532, the high K concentration has a catalytic effect on hemicellulose decomposition. Thus, the CO_2 shoulder peak from hemicellulose (at ~ 14 min) occurs at lower temperatures compared to other blends. The CH_4 release profile arises from the cracking of methoxyl groups in lignin and ceases after active pyrolysis with M532 as an outlier. The NH_3 (a NO_x precursor) profile diminishes with increasing amounts of M010 in the blends, while CO emitted during cellulose devolatilization is proportional to the M010 concentrations. The second peak of CO_2 and CO visible at ~ 44 min corresponds to the carbonate decomposition region. The

evolution of CO beyond 700 °C is from the gasification of char in presence of CO_2 .

3.4 Scaling effect during biomass pyrolysis

To the extent of the authors' knowledge, the literature has rarely investigated whether the process characteristics and biochar properties usually studied via analytical pyrolysis (sample mass < 10 mg) at a particular HTT of lignocellulosic biomass are comparable to pyrolysis investigations using larger sample masses that induce heat and mass transfer effects. Among the BM, M010 is used for this preliminary scaling investigation since it has relatively lower ash and paramagnetic impurities that can influence the thermal gradient within the substrate during pyrolysis and the ^{13}C ssNMR analysis, respectively at increasing mass scales. Figure 4 shows the rate of mass loss and heat flow during the pyrolysis of M010 at different mass scales between 5 and 500 mg in the TGA. In the normalized DTG curve, with increasing scales, the max peak devolatilization rate increases and the contribution of total mass loss shifts towards higher temperatures. This stems from the increased contact of evolved volatiles with the substrate leading to exothermic char-forming reactions. This is also seen in the total HoP (Fig. S15 in SM) which tends to shift from endothermic to exothermic after scl_75. There is also a statistically significant difference in heat flow between different scales (Sect. 4.4 in SM).

The distribution of carbon moieties – aryl, alkyl, and carbonyl – based on CP and DP spectra, in the biochar produced in the TGA at different scales (at constant HTT 650 °C) are presented in Fig. 5 while Fig. 6 shows the relative observable carbon and total carbon in the biochar. The SSB occur in the CP and DP (Figs. S16 and S17 in

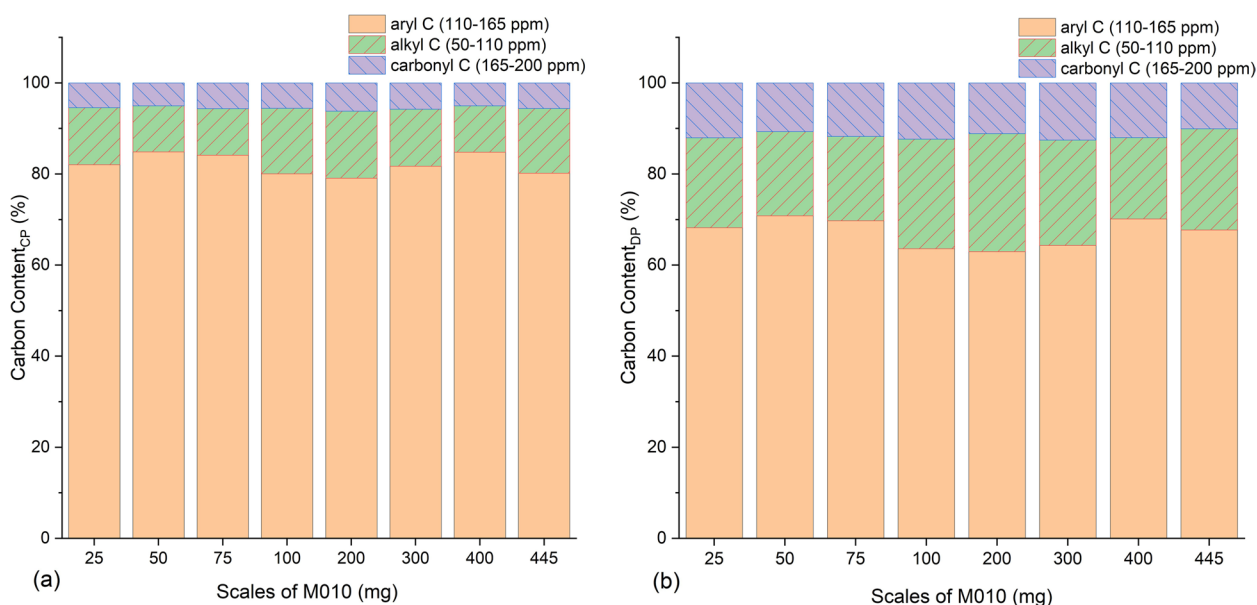


Fig. 5 The biochar produced from different mass scales of pyrolysis of M010 in TGA showing the distribution of carbon content (%) in biochar as a percentage of ^{13}C NMR (a) cross polarization (CP) signal intensity and (b) direct polarization (DP)

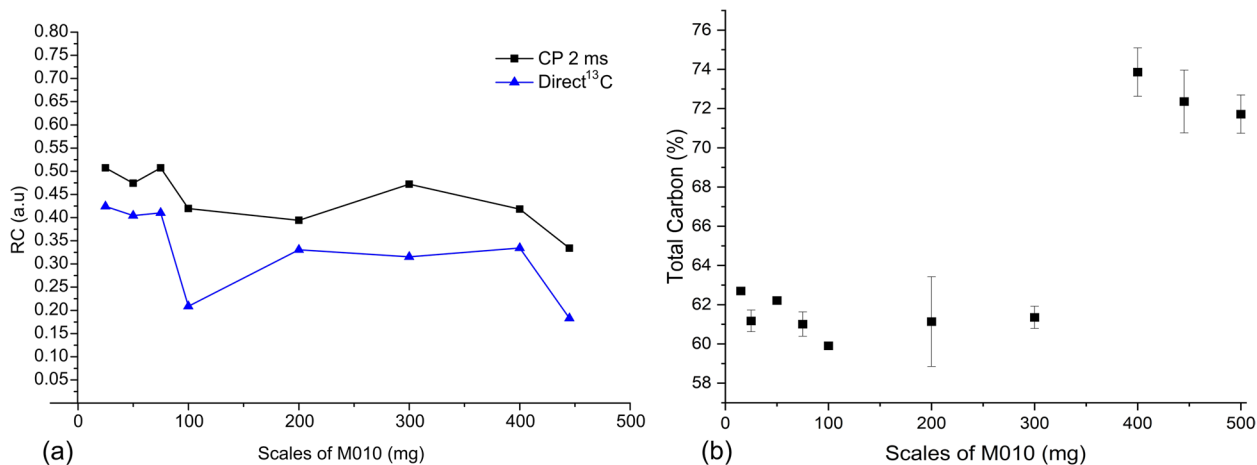


Fig. 6 Biochar derived from M010 at different mass scales (mg) showing a) the relative observable carbon (RC) in arbitrary units (a.u) and b) total carbon content (%)

SM) due to insufficient MAS compared to the anisotropy of the chemical shift signals in biochar. Furthermore, the non-protonated fraction of C has not been isolated from the total C signal and measured separately using the method of DP/MAS with dipolar dephasing of ^1H from carbon nuclei. Hence, the determination of C moieties based on CP and DP here is only semi-quantitative. The CP and DP spectra show aryl resonance at ~ 130 ppm. The assigned aryl C region can also include phenols and aromatic O–C such as those in recalcitrant lignin. The aryl C estimated by CP/MAS is higher than DP/MAS at

all mass scales due to the stronger spillover of alkyl bands ($\text{sp}^3 \text{O} - \text{C} - \text{O}$) to the aromatic region in biochar carbon matrix with higher protonation (H/C molar ratio). However, it can be observed that the aryl C content does vary with scales in the same pattern in both CP and DP, with the lowest values at scl_100 and scl_200. The relative observable carbon tends to decrease with scale in both CP and DP spectra despite DP directly measuring the nuclear spin polarization of the C nuclei. This could hint at the enrichment of paramagnetic impurities such as Fe, K and Mg that changes with scales. The total carbon

seems to increase by more than ~16% from scl_400. It can be hypothesized that for a given pyrolysis reactor type (such as TGA) and HTT, there is a certain mass scale beyond which M010 show a predominant influence of char forming secondary reactions that maximize its exothermicity with carbon content and its distribution in the derived biochar also dependent on mass scales. The determination of the correlation between these secondary reactions and carbon content deems further structural analyses such as X-ray diffraction, N₂ physisorption, and Raman spectroscopy, which are beyond the scientific and financial scope of this study but explored in a follow-up investigation.

4 Conclusions

Mineral and/or ash-rich biomass such as sewage sludge from WWT constitutes a large proportion of the influx to solid waste treatment facilities in urban areas, especially in emerging economies. Their combined conversion into biochar for carbon sequestration can support local waste management and global decarbonization efforts. To this end, the biochar derived from the co-pyrolysis of digested sewage sludge with refuse lignocellulosic waste (banana peduncle) and anaerobic digestate from organic waste processing facilities are investigated in a lab-scale reactor to understand their capacities for carbon sequestration in soils. From the same materials and their blends, biochar was also produced and studied in a TGA/DSC-FTIR analyser to investigate the process characteristics and possible scaling effects. The major conclusions are summarized as follows:

- i. Yield, HPT and thermal oxidative recalcitrance of biochar during lab-scale co-pyrolysis are independent of blending ratios of M100, M010 and M001. Compared to parent feedstock, blended MWB tends to show their characteristics during pyrolysis due to synergy amongst the biomass components.
- ii. Co-pyrolysis of these MWB at 500 °C for 60 min was sufficient to depolymerize the lignocellulose. However, complete carbonization at this HTT is not achieved, which can be mitigated by raising the residence time in the lab-scale reactor. However, HTT above 500 °C can render the process energy intensive and increase HM enrichment in biochar.
- iii. Compared to SSW-derived biochar, better carbonization and reduced ashing were seen in the biochar when SS was co-pyrolyzed with other MWB. Amongst the biochars produced in lab-scale at 500 °C, B550 and B514 are the most carbonized (class 2 according to IBI). Except for B505 and B100, the biochar can be deposited in acidic soils

due to the presence of NPK nutrients, and hydrophilic DOC.

- iv. The general pyrolysis emission profiles follow the order CO₂ > CH₄ > CO > NH₃. When the proportion of M010 in MM is increased, peak temperatures and NH₃ emissions during co-pyrolysis under 500 °C are lowered. The addition of M010 improved the exothermicity of active pyrolysis of M100.
- v. To minimize energy consumption, CO and NH₃ emissions, and HM aggregation the optimal temperature for co-pyrolysis is 500 °C. For the first time, it is experimentally proven that the scaling effect during analytical pyrolysis influences the char formation reactions, the carbon distribution (aryl, alkyl, and carbonyl C) and the total carbon content in biochar. For future modelling of pyrolysis systems, especially to forecast the heat of pyrolysis, this scaling effect must be considered.

The investigation confirmed a maximum carbon sequestration potential (up to 0.22 kg CO₂ kg⁻¹ biomass) of biochar derived from co-pyrolysis of SSW with other MWB, thereby aiding the solid waste management efforts in emerging urban areas such as Chennai. Further in-depth investigations into the plant-available heavy metals in this biochar (sequential speciation), long-term field tests in soil, technology costing, and the emission profile during pyrolysis scale-up are necessary. In the follow-up studies, authors explore the influence of scaling effects on analytical pyrolysis and biochar production from these MWB using an industrial-scale pyrolysis reactor in Chennai.

Supplementary Information

The online version contains supplementary material available at <https://doi.org/10.1186/s42834-023-00176-9>.

Additional file 1.

Acknowledgements

- PD Dr. Stefan Dultz and Roger-Michael Klatt (retired) at the Institute of Soil Science, Leibniz University Hannover (LUH)
- Benjamin Grüger at the Institute for Sanitary Engineering and Waste Management (ISAH), LUH

Authors' contributions

Conceptualization and methodology – R.R.N, D.W; Experiments – R.R.N, P.K, A.M, J.L, A.E.T, S.V.S; Lab-scale production of biochar: R.R.N (also experimental design), N.R, S.G; Data Curation & Visualization: R.R.N; Formal analysis: R.R.N; Writing (original draft) – R.R.N; Writing (review and editing): R.R.N, P.K, A.M, A.E.T, M.S, J.P, D.W; Supervision: D.W, J.P; Funding & Resources: D.W, S.V.S; Administration: D.W, S.V.S; All authors have read and agreed to the published version of the manuscript.

Funding

Open Access funding enabled and organized by Projekt DEAL. - Bundesministerium für Bildung und Forschung (BMBF) and Indo-German Science and Technology Center (IGSTC) under the project PYRASOL (FKZ 01DQ18001A). - PhD Fellowship German Academic Exchange Service (DAAD) Program number 57381412. - Deutsche Forschungsgemeinschaft (DFG, German Research Foundation) under the project BI1708/5 -1.

Availability of data and materials

Available upon request.

Declarations

Competing interests

The authors declare no relevant financial or any other competing interests in the content of this article.

Author details

¹Institute of Sanitary Engineering and Waste Management, Leibniz University of Hannover, 30167 Hannover, Germany. ²Institute of Physical Chemistry and Electrochemistry, Leibniz University of Hannover, 30167 Hannover, Germany. ³Institute of Organic Chemistry and Centre of Biomolecular Drug Research, Leibniz University of Hannover, 30167 Hannover, Germany. ⁴Institute of Plastics and Circular Economy, Leibniz University of Hannover, 30823 Garbsen, Germany. ⁵Institute of Botany, Leibniz University of Hannover, 30419 Hannover, Germany. ⁶Environmental Engineering Department, Central Leather Research Institute, Chennai 600020, India.

Received: 17 January 2023 Accepted: 11 April 2023

Published online: 24 April 2023

References

- UN. The Sustainable Development Goals Report 2022. New York: United Nations; 2022.
- Van Caneghem J, Van Acker K, De Greef J, Wauters G, Vandecasteele C. Waste-to-energy is compatible and complementary with recycling in the circular economy. *Clean Technol Environ*. 2019;21:925–39.
- Jindo K, Audette Y, Higashikawa FS, Silva CA, Akashi K, Mastrodonato G, et al. Role of biochar in promoting circular economy in the agriculture sector. Part 1: A review of the biochar roles in soil N, P and K cycles. *Chem Biol Technol Ag*. 2020;7:15.
- Singh V, Phuleria HC, Chandel MK. Estimation of energy recovery potential of sewage sludge in India: Waste to watt approach. *J Clean Prod*. 2020;276:122538.
- Kaza S, Yao LC, Bhada-Tata P, Van Woerden F. What a waste 2.0: a global snapshot of solid waste management to 2050. Washington, DC: World Bank; 2018.
- Dolla T, Laishram B. Effect of energy from waste technologies on the risk profile of public-private partnership waste treatment projects of India. *J Clean Prod*. 2021;284:124726.
- Singh V, Phuleria HC, Chandel MK. Unlocking the nutrient value of sewage sludge. *Water Environ J*. 2022;36:321–31.
- Gao N, Kamran K, Quan C, Williams PT. Thermochemical conversion of sewage sludge: A critical review. *Prog Energy Combust*. 2020;79:100843.
- Lin Y, Liao Y, Yu Z, Fang S, Lin Y, Fan Y, et al. Co-pyrolysis kinetics of sewage sludge and oil shale thermal decomposition using TGA–FTIR analysis. *Energy Convers Manage*. 2016;118:345–52.
- Manara P, Zabaniotou A. Towards sewage sludge based biofuels via thermochemical conversion – A review. *Renew Sust Energy Rev*. 2012;16:2566–82.
- Wang GY, Dai YJ, Yang HP, Xiong QG, Wang KG, Zhou JS, et al. A Review of recent advances in biomass pyrolysis. *Energy Fuel*. 2020;34:15557–78.
- Zuhara S, Mackey HR, Al-Ansari T, McKay G. A review of prospects and current scenarios of biomass co-pyrolysis for water treatment. *Biomass Convers Bior*. 2022; doi: <https://doi.org/10.1007/s13399-022-03011-0>.
- Wang CX, Bi HB, Lin QZ, Jiang XD, Jiang CL. Co-pyrolysis of sewage sludge and rice husk by TG-FTIR-MS: Pyrolysis behavior, kinetics, and condensable/non-condensable gases characteristics. *Renew Energy*. 2020;160:1048–66.
- Schnell M, Horst T, Quicker P. Thermal treatment of sewage sludge in Germany: A review. *J Environ Manage*. 2020;263:110367.
- Nair RR, Mondal MM, Srinivasan SV, Weichgrebe D. Biochar synthesis from mineral- and ash-rich waste biomass, part 1: investigation of thermal decomposition mechanism during slow pyrolysis. *Materials*. 2022;15:4130.
- Wu WX, Mei YF, Zhang L, Liu RH, Cai JM. Effective Activation Energies of Lignocellulosic Biomass Pyrolysis. *Energy Fuel*. 2014;28:3916–23.
- Anca-Couce A, Berger A, Zobel N. How to determine consistent biomass pyrolysis kinetics in a parallel reaction scheme. *Fuel*. 2014;123:230–40.
- Permanyer A, Douifi L, Lahcini A, Lamontagne J, Kister J. FTIR and SUVF spectroscopy applied to reservoir compartmentalization: a comparative study with gas chromatography fingerprints results. *Fuel*. 2002;81:861–6.
- Brunauer S, Emmett PH, Teller E. Adsorption of gases in multimolecular layers. *J Am Chem Soc*. 1938;60:309–19.
- Nair RR, Mondal MM, Weichgrebe D. Biochar from co-pyrolysis of urban organic wastes—investigation of carbon sink potential using ATR-FTIR and TGA. *Biomass Convers Bior*. 2022;12:4729–43.
- Fung BM, Khitrin AK, Ermolaev K. An improved broadband decoupling sequence for liquid crystals and solids. *J Magn Reson*. 2000;142:97–101.
- Conte P, Spaccini R, Piccolo A. State of the art of CPDAS 13C-NMR spectroscopy applied to natural organic matter. *Prog Nucl Mag Res Sp*. 2004;44:215–23.
- Wang XB, Deng SH, Tan HZ, Adeosun A, Vujanovic M, Yang FX, et al. Synergistic effect of sewage sludge and biomass co-pyrolysis: A combined study in thermogravimetric analyzer and a fixed bed reactor. *Energy Convers Manage*. 2016;118:399–405.
- Yin Q, Liu M, Ren H. Biochar produced from the co-pyrolysis of sewage sludge and walnut shell for ammonium and phosphate adsorption from water. *J Environ Manage*. 2019;249:109410.
- Xiao X, Chen ZM, Chen BL. H/C atomic ratio as a smart linkage between pyrolytic temperatures, aromatic clusters and sorption properties of biochars derived from diverse precursory materials. *Sci Rep-Uk*. 2016;6:22644.
- Schimmelpfennig S, Glaser B. One step forward toward characterization: some important material properties to distinguish biochars. *J Environ Qual*. 2012;41:1001–13.
- Enders A, Hanley K, Whitman T, Joseph S, Lehmann J. Characterization of biochars to evaluate recalcitrance and agronomic performance. *Biore-source Technol*. 2012;114:644–53.
- Bakshi S, Banik C, Laird DA. Estimating the organic oxygen content of biochar. *Sci Rep-Uk*. 2020;10:13082.
- Isaeva VI, Vedenyapina MD, Kurmysheva AY, Weichgrebe D, Nair RR, Nguyen NPT, et al. Modern carbon-based materials for adsorptive removal of organic and inorganic pollutants from water and wastewater. *Molecules*. 2021;26:6628.
- Gbouri I, Yu F, Wang X, Wang J, Cui X, Hu Y, et al. Co-Pyrolysis of Sewage sludge and wetland biomass waste for biochar production: behaviors of phosphorus and heavy metals. *Int J Env Res Pub He*. 2022;19:2818.
- Lehmann J, Joseph S. Biochar for environmental management science, technology and implementation. 2nd ed. London: Routledge; 2015.
- Ruzickova J, Koval S, Raclavska H, Kucbel M, Svedova B, Raclavsky K, et al. A comprehensive assessment of potential hazard caused by organic compounds in biochar for agricultural use. *J Hazard Mater*. 2021;403:123644.
- Spokas KA. Review of the stability of biochar in soils: predictability of O:C molar ratios. *Carbon Manag*. 2010;1:289–303.
- Budai A, Zimmerman AR, Cowie AL, Webber JBW, Singh BP, Glaser B, et al. Biochar carbon stability test method: an assessment of methods to determine biochar carbon stability. International Biochar Initiative. 2013.
- Kong SH, Loh SK, Bachmann RT, Zainal H, Cheong KV. Palm kernel shell biochar production, characteristics and carbon sequestration potential. *J Oil Palm Res*. 2019;31:508–20.
- Cayuela ML, Jeffery S, van Zwielen L. The molar H:Corg ratio of biochar is a key factor in mitigating N₂O emissions from soil. *Agr Ecosyst Environ*. 2015;202:135–8.
- Waqas M, Khan S, Qing H, Reid BJ, Chao C. The effects of sewage sludge and sewage sludge biochar on PAHs and potentially toxic element bioaccumulation in *Cucumis sativa* L. *Chemosphere*. 2014;105:53–61.

38. Jin JW, Li YN, Zhang JY, Wu SC, Cao YC, Liang P, et al. Influence of pyrolysis temperature on properties and environmental safety of heavy metals in biochars derived from municipal sewage sludge. *J Hazard Mater*. 2016;320:417–26.
39. Wang ZP, Xie LK, Liu K, Wang J, Zhu HN, Song Q, et al. Co-pyrolysis of sewage sludge and cotton stalks. *Waste Manage*. 2019;89:430–8.
40. Zhao ZD, Wu QQ, Nie TT, Zhou WJ. Quantitative evaluation of relationships between adsorption and partition of atrazine in biochar-amended soils with biochar characteristics. *Rsc Adv*. 2019;9:4162–71.
41. Wang T, Chen YC, Li JP, Xue YJ, Liu JX, Mei M, et al. Co-pyrolysis behavior of sewage sludge and rice husk by TG-MS and residue analysis. *J Clean Prod*. 2020;250:119557.
42. Liu TZ, Liu BY, Zhang W. Nutrients and heavy metals in biochar produced by sewage sludge pyrolysis: its application in soil amendment. *Pol J Environ Stud*. 2014;23:271–5.
43. EBC. European Biochar Certificate - Guidelines for a Sustainable Production of Biochar. Arbaz: European Biochar Certificate; 2016.
44. Solar J, de Marco I, Caballero BM, Lopez-Urionabarrenechea A, Rodriguez N, Agirre I, et al. Influence of temperature and residence time in the pyrolysis of woody biomass waste in a continuous screw reactor. *Biomass Bioenerg*. 2016;95:416–23.
45. Lv GJ, Wu SB. Analytical pyrolysis studies of corn stalk and its three main components by TG-MS and Py-GC/MS. *J Anal Appl Pyrol*. 2012;97:11–8.
46. Zhang SP, Dong Q, Zhang L, Xiong YQ. Effects of water washing and torrefaction on the pyrolysis behavior and kinetics of rice husk through TGA and Py-GC/MS. *Bioresource Technol*. 2016;199:352–61.
47. Singh B, Camps-Arbestain M, Lehmann J. *Biochar: a guide to analytical methods*. Boca Raton: CRC Press; 2017.
48. Calvelo Pereira R, Kaal J, Camps Arbostain M, Pardo Lorenzo R, Aitkenhead W, Hedley M, et al. Contribution to characterisation of biochar to estimate the labile fraction of carbon. *Org Geochem*. 2011;42:1331–42.
49. Xu X, Zhao Y, Sima J, Zhao L, Masek O, Cao X. Indispensable role of biochar-inherent mineral constituents in its environmental applications: A review. *Bioresource Technol*. 2017;241:887–99.
50. Tomczyk A, Sokolowska Z, Boguta P. Biochar physicochemical properties: pyrolysis temperature and feedstock kind effects. *Rev Environ Sci Bio*. 2020;19:191–215.
51. Carrier M, Hardie AG, Uras U, Gorgens J, Knoetze J. Production of char from vacuum pyrolysis of South-African sugar cane bagasse and its characterization as activated carbon and biochar. *J Anal Appl Pyrol*. 2012;96:24–32.
52. Tate RL. *Soil Microbiology*. 3rd ed. Hoboken: John Wiley & Sons, Inc.; 2020.
53. Zhao SL, Liu M, Zhao L, Lu JH. Effects of organic and inorganic metal salts on thermogravimetric pyrolysis of biomass components. *Korean J Chem Eng*. 2017;34:3077–84.
54. Zhang J, Zhao R, Du YY, Chen L, Chen ZZ, Xiao N, et al. Study on the co-pyrolysis characteristics of sewage sludge and wood powder and kinetic analysis. *Biomass Convers Bior*. 2022.
55. Hameed Z, Aman Z, Naqvi SR, Tariq R, Ali I, Makki AA. Kinetic and thermodynamic analyses of sugar cane bagasse and sewage sludge co-pyrolysis process. *Energy Fuel*. 2018;32:9551–8.
56. Naqvi SR, Hameed Z, Tariq R, Taqvi SA, Ali I, Niazi MBK, et al. Synergistic effect on co-pyrolysis of rice husk and sewage sludge by thermal behavior, kinetics, thermodynamic parameters and artificial neural network. *Waste Manage*. 2019;85:131–40.

Publisher's Note

Springer Nature remains neutral with regard to jurisdictional claims in published maps and institutional affiliations.

Ready to submit your research? Choose BMC and benefit from:

- fast, convenient online submission
- thorough peer review by experienced researchers in your field
- rapid publication on acceptance
- support for research data, including large and complex data types
- gold Open Access which fosters wider collaboration and increased citations
- maximum visibility for your research: over 100M website views per year

At BMC, research is always in progress.

Learn more biomedcentral.com/submissions

